IEEE Access
Multidisciplinary | Rapid Review | Open Access Journal

Received February 21, 2021, accepted March 7, 2021, date of publication March 17, 2021, date of current version March 25, 2021.

Digital Object Identifier 10.1109/ACCESS.2021.3066525

A 2 × 3 Reconfigurable Modes Wide Input Wide Output Range DC-DC Power Converter

M. ABU BAKAR[1], M. FARHAN ALAM[1], MATS WÅRDEMARK[2], AND KENT BERTILSSON[1], (Member, IEEE)

[1]Department of Electronics Design, Mid Sweden University, 85170 Östersund, Sweden
[2]Powerbox International AB, 646 35 Gnesta, Sweden

Corresponding author: M. Abu Bakar (MuhammadAbu.Bakar@miun.se)

ABSTRACT There is an increasing demand for efficient and low-profile power converters in almost all industrial applications. Some require stable performance over a wide range of input voltages, whereas others require converters with a stable performance over a wide range of output voltages. In this regard, little work has been done to combine both requirements into one solution. This work suggests a unique solution that addresses both requirements at once. A power converter with 2×3 reconfigurable modes has been presented, able to operate with DC gains of 1, 2 and 4, which can be further extended to 8. The converter shows stable performance for the extended range of both input and output voltage. The flexible reconfigurable feature of the proposal can be applied in a variety of applications. Two reconfigurable modes on the input side can be configured following the variation in the line voltage to maintain a stable performance, and three reconfigurable modes for the output voltage, which raises the output voltage from 24V to 48V and 96V. The proposal is applied in an example application of a phase shifted full bridge converter. The converter is characterized for $V_{in} = 100\text{-}400V_{dc}$, $P_{out} = 1kW$.

INDEX TERMS Wide range power converters, reconfigurable converters, flexible converter, ZVS converters, wide input range, PSFB converter, medium power, series transformer, wide output.

I. INTRODUCTION

Wide range power converters are receiving attention in a broad range of industrial applications, like server stations, DC grids, photovoltaics, electric vehicles and supercapacitors. Some require a power converter with the capability to handle wide variations in the input voltage, like photovoltaic applications, whereas others require a converter capable of handling wide variations in the output voltage, like charging of batteries/supercapacitors. Photovoltaic/server station applications need wide input range converters at a fixed output voltage, whereas battery/supercapacitor charging applications need wide output range converters at a fixed input voltage. An extensive work [1]–[8] is progressing in the power electronics industry to meet the requirements to some extent. The focus has been on either extending the range of input voltage or extending the range of output voltage. The literature [9]–[13] provides a solution for server power applications: to reduce the size of the link capacitors during hold-up time. The performance of the converter is optimised only for the nominal operating range. This narrows the scope of the proposal. The main constraint in extending the range of input voltage is the reduction of the operational duty cycle with the increase in line voltage. More circulating current flows in the freewheeling interval adds more conduction loss. In [14], an adapted control strategy has been presented to minimize circulation current loss. However, it reduces losses only under low power conditions and makes the design complex. The authors [15] reduce the conduction loss by adding a boost capacitor, however, it cuts the range of zero voltage switching. The literature [4]–[6], [16] reports an extended range of input voltage for photovoltaic and EV applications. Although they report stable performance over the extended range of the input voltage, the output voltage remains fixed.

Similarly, the proposals [1]–[3], [17]–[19] report stable performance over the extended range of the output voltage, however, the input voltage remains fixed. The most common approach for the extended range of voltage gain is a frequency modulated LLC power converter. LLC converters show optimum performance when operating at the resonant frequency,

The associate editor coordinating the review of this manuscript and approving it for publication was Meng Huang.

the switching frequency has to swing in a wide range to achieve extended voltage gain, this results in degraded overall performance [4]. Moreover, the voltage regulation of LLC converters is load-dependent and affected by circuit parameters like resonant capacitance and magnetizing/resonant inductance [3]. The variable frequency operation further adds complexity regarding EMI. The other traditional solution used to obtain a wide range of output voltage is the bench type variable output power supplies. These solutions could be linear power supplies or switch-mode power supplies. However, none of the solutions meets the present requirement because of their bulkiness and lower efficiency. To meet the requirement of a wide range of output voltage, multiple power converters are usually stacked together, which increases the cost and complexity of the system [12]. Moreover, it degrades the reliability and efficiency of the overall system.

This proposal presents a novel concept to extend the range of both sides as a single reconfigurable solution. By using the reconfigurable characteristics of the proposed converter along with the requirement of the intended application, the range of either side can be extended while keeping the performance stable. This work is an extension of previous work [13], [20], [21], where the solutions for extending both ranges have been separately discussed. By combining both solutions, this work introduces a novel concept of a five distinct mode isolated power converter. This one size fits all flexible solution can be implemented either in wide input-range applications or in wide-output range applications. This work focuses on a complete system, however, for simplicity, the discussion has been kept consistent with previous work. The simplified block diagram of the proposed concept is shown in Fig. 1. There are 2 × 3 distinct modes, i.e., modes 1-2 on the input side and modes 3-5 on the output side. The converter can be configured to either set of input/output modes manually or by pre-programming a certain limit. Generally, power converters are designed for nominal operating conditions, the performance degrades beyond nominal conditions. The reduction of the duty cycle with the increase in line voltage is the main cause of performance degradation, due to the flow of more circulating current and increased ripple current. In the proposed converter, instead of reducing the duty cycle, the effective gain of the converter is adjusted to keep the operational duty cycle high for a wider range of input voltage to maintain a stable performance. For the extended range of output, instead of changing the switching frequency like an LLC resonant converter, the output voltage can be raised from base voltage X volt to 2X volt, to 4X volt or 8X volt. The proposal has been verified in an example application of a phase shifted full bridge (PSFB) converter, where the converter is characterized for an input voltage of 100-400V and up to the load power of 1kW. To simplify, both wide input and wide output characteristics have been investigated separately.

The main advantages of the proposal are (1) a unique one size fits all solution for both wide input range applications and wide output range applications while keeping the performance stable, (2) the flexible reconfigurable structure simplifies implementation for a variety of applications, (3) the gain of the converter can be raised to eight and (4) the use of series transformers simplifies heat management.

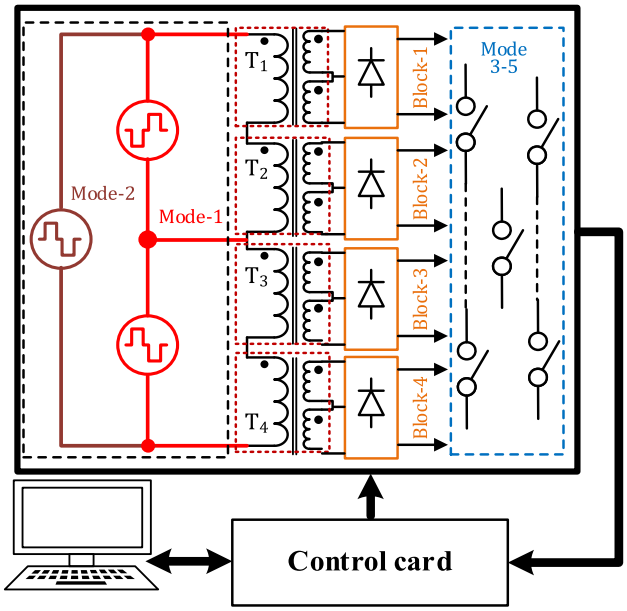

FIGURE 1. Block diagram of the proposed converter, showing five reconfigurable modes, two on the input side and three on the output side.

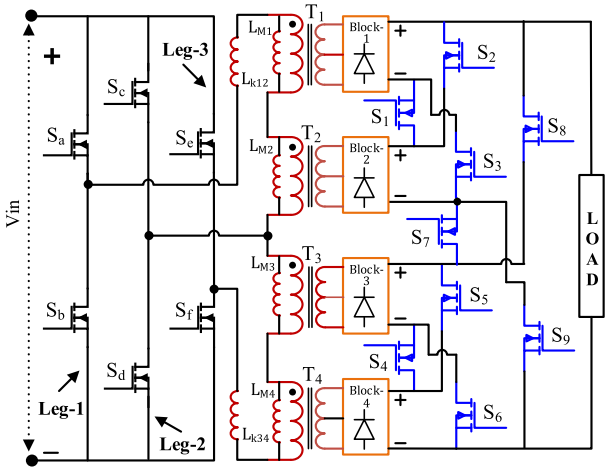

FIGURE 2. Simplified circuit diagram of the converter showing key circuit elements of each section.

II. CIRCUIT DESCRIPTION

The main circuit diagram of the converter is shown in Fig. 2. The full circuit can be divided into four main sections, power drive section, power transfer section, the rectification section and the output control section. The power drive section comprises of six power devices S_a-S_f, which are arranged to drive power making three legs on the primary side. As shown in the switching diagram Fig. 4, in primary mode-1, the devices of both leg-1 and leg-3 operate in phase, whereas in mode-2, leg-2 stays neutral. The inductors L_{k12} and L_{k34} are the sums of

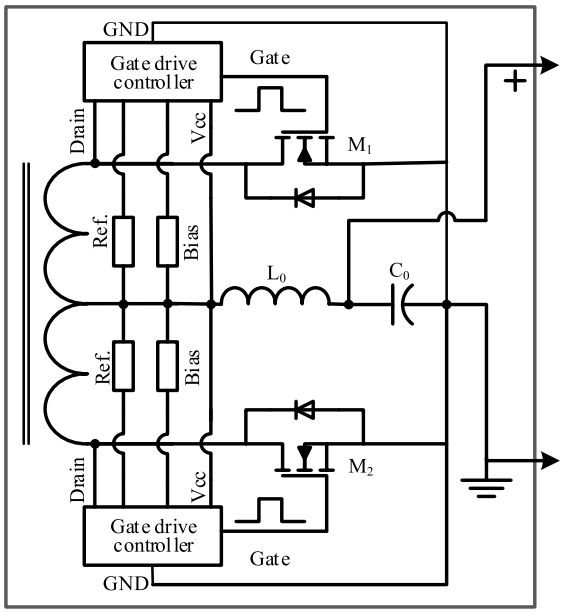

FIGURE 3. Synchronous rectification of one of the output blocks along with proportional gate drive controller.

the intrinsic leakage inductance of transformers $T_1 - T_2$ and the transformers $T_3 - T_4$ respectively. Along with intrinsic output capacitance of power devices, the inductors

L_{k12} and L_{k34} resonate to obtain soft switching of power devices. The power transfer section contains four transformers, which transfer power from the primary side to the secondary side, and provides isolation between the two sides. Each transformer consists of the same number of primary turns N_P and secondary turns N_S. The rectification section independently rectifies the secondary winding voltage of each transformer and makes four isolated blocks of the output voltage. Each block rectifies the respective secondary winding voltage employing synchronous rectification by using the proportional gate drive technique. This technique eliminates the need for an external biasing supply for the gate driver, thus makes it possible to build an electrically isolated rectified voltage for each transformer. A circuit diagram of one of the output blocks is shown in Fig. 3. Each block contains two MOSFETs along with independent gate drive controllers for synchronous rectification and the filtering elements capacitor/inductor. The output control section consists of nine active devices S_1-S_9. These devices are arranged to configure the output voltage in any of the three possible modes, that is mode-3 to mode-5 on the output side. It means the provision of nine active switches aligns blocks in series, parallel or a combination of series/ parallel.

As mentioned, the proposed converter has 2 × 3 reconfigurable modes, i.e., two on the input side and three on the output side. This makes five distinct operational modes. The converter works differently in each mode. To simplify the analysis, mode-3 has been considered as the default configuration of the output control section, where all blocks connect in parallel. The switching control signals along with key waveforms, like transformer primary voltage/current, are

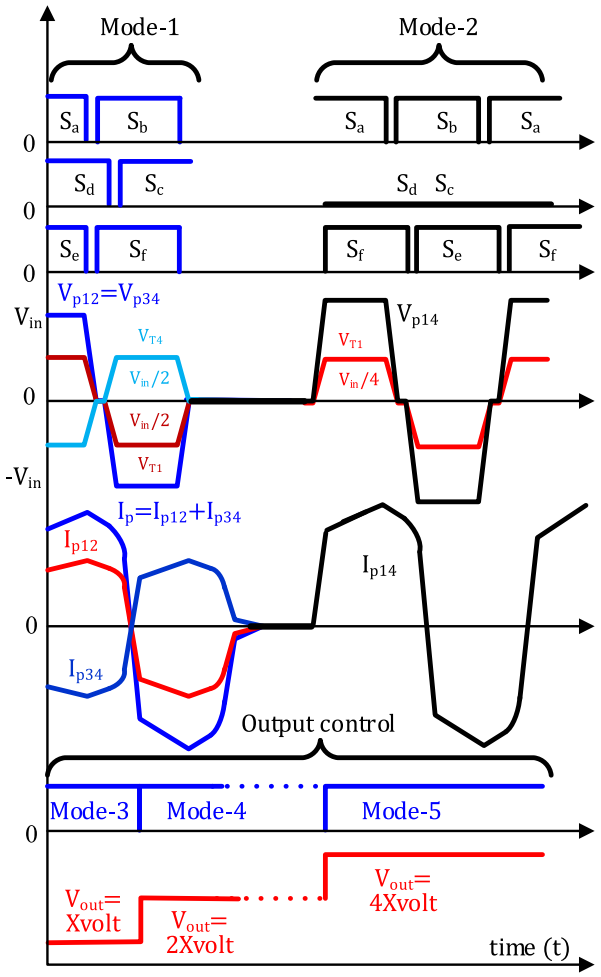

FIGURE 4. Device switching control along with key switching waveforms for operational modes 1-5.

shown in Fig. 4 [22]–[26]. The following is an explanation of how the proposed converter works in order to extend both ranges. For simplicity, the discussion has been categorized into two sections.

III. EXTENSION OF THE INPUT RANGE

A. OPERATION OF MODE-1/MODE-3

In mode-1, all six power devices take part in power conversion. One device from each leg contributes alternatively in a half-period of a cycle. As seen in Fig. 4, both outer legs are out of phase with leg-2. Leg-2 clamps input voltage on the common point to V_{in} and zero in alternate half cycles. This connects a pair of series-connected transformers $T_1 - T_2$ and $T_3 - T_4$ in parallel. The voltage stress on each transformer in that case is $V_{p12}/2$, the primary current also follows two paths i.e., I_{p12} through transformers $T_1 - T_2$ and I_{p34} through transformers $T_3 - T_4$. After passing through synchronous rectification and filtering elements, the rectification section prepares four isolated blocks of the output voltage. To configure them in parallel, switches S_2, S_5 and S_8 connect positive terminals and switches S_3, S_6, and S_9 connect negative

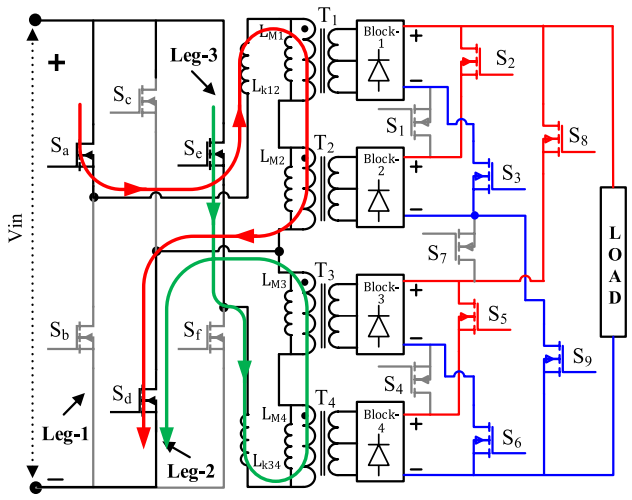

FIGURE 5. Status of devices/switches and the flow of current in a half-cycle of the period during the operation of the converter in mode-1/mode-2.

terminals. This parallel configuration is finally applied to the load. Fig. 5 shows the status of devices on the primary side and the status of switches on the secondary side for one of the half-cycles. In the other half-cycle, the other group of primary devices, i.e., S_b, S_c, and S_f, become active, whereas on the secondary side, which is the default configuration, the same set of switches remains active. Both primary current I_{p12} and I_{p34} can be determined as

$$I_{p12} = I_{p34} = \left\{ \left(\frac{V_{in} - n_{ef\_1} V_{out}}{2L_{m\_1} + 2L_{k\_1} + \left(n_{ef\_1}\right)^2 L_{o\_T}} \right) + I_{Lo\_T}/n_{ef\_1} \right\} \quad (1)$$

where V_{in} is the input voltage, V_{out} is the output voltage, L_{m_1} and L_{k_1} are respectively the effective magnetizing/leakage inductances, L_{o_T} is the total output filter inductance, and I_{Lo_T} is the total load current. The effective turn ratio is defined as $n_{ef\_1} = \frac{(V_{in}/2)}{V_{out}} = \frac{N_p}{N_s}$, where $N_p N_s$ are the number of primary and secondary turns respectively. The output voltage of the converter at the terminals of the load is determined as

$$V_{out}(mode_{1/3}) = 2D_{eff} \frac{N_s}{N_p} \left(\frac{V_{in}}{2} \right) \quad (2)$$

The effective duty cycle D_{eff} is defined as $D_{eff} = D - \left(D_{loss} + \varphi_{shift}\right)$, where D is the duty cycle.

B. OPERATION OF MODE-2/MODE-3

As shown in Fig. 4, the operation of the converter in mode-2 differs in such a way that the devices of leg-2 remain inactive and the converter operates as a traditional phase shifted full bridge converter. The outer two legs take part in the transfer of power. The power is transferred alternatively through a diagonal pair of devices $S_a - S_f$, and $S_b - S_e$. It connects the primary winding of all four transformers in series. The input voltage V_{p14} is divided between four transformers and the voltage on each transformer is reduced to $V_{in}/4$, and the same amount of primary current I_{p14}, flows through each transformer. The primary current in mode-2/ mode-3 can be determined as

$$I_{p14} = \left\{ \left(\frac{V_{in} - n_{ef\_2} V_{out}}{L_{m\_2} + L_{k\_2} + \left(n_{ef\_2}\right)^2 L_{o\_T}} \right) + I_{Lo\_T}/n_{ef\_2} \right\} \quad (3)$$

where L_{m_2} and L_{k_2} are the effective magnetizing/leakage inductances respectively. The effective turn ratio is $n_{ef\_2} = \frac{(V_{in}/4)}{V_{out}} = \frac{N_p}{N_s}$. The output voltage of the converter for this configuration can be determined as

$$V_{out}(mode_{2/3}) = 2D_{eff} \frac{N_s}{N_p} \left(\frac{V_{in}}{4} \right) \quad (4)$$

IV. EXENSTION OF THE OUTPUT RANGE

A. OPERATION OF MODE-4

This mode relates to the output control section, and can be made active while the primary side is either in mode-1 or in mode-2. Therefore, only the operational status of the output control section will be discussed. This mode first configures two blocks in series and then connect them in parallel. As seen in Fig. 6(a), switch S_1 configures block-1 and block-2 in series, and switch S_4 configures block-3 and block-4 in series. The switches S_8 and S_9 connect this series combination in parallel. This means that the voltage that appears on the load is $V_{load} = \left(V_{block\_1} + V_{block\_2}\right) \parallel \left(V_{block\_3} + V_{block\_4}\right)$. This doubles the output voltage of the default mode-3. The output voltage can be determined by considering any of the operational modes on the primary side. For the primary section configured in mode-1, the output voltage of the converter in mode-4 is

$$V_{out}(mode_{1/4}) = \left[2D_{eff} \frac{N_s}{N_p} \left(\frac{V_{in}}{2} \right) \right] \times 2 \quad (5)$$

In mode-4, a series-connected pair of output filter inductors appears in parallel to the load. The primary current can be determined either by (1) or (3) and by considering the total value of the output filter inductance in this mode.

B. OPERATION OF MODE-5

This mode also relates to the output control section. It configures all blocks of the output voltage in series. This mode can also be made active regardless of the operational status of the primary section, i.e., either mode-1 or mode-2. As shown in Fig. 5(b), three switches S_1, S_4 and S_7 take part in arranging all blocks in series. The three switches involved connect positive and negative terminals and thus the load is provided with the series configuration of all blocks. This means the output voltage is four times higher compared to the default configuration of the output control section, i.e., mode-3. Similar to mode-4, the output voltage of the converter can be determined by considering either of the operational modes on the primary side. For example, the output voltage of the

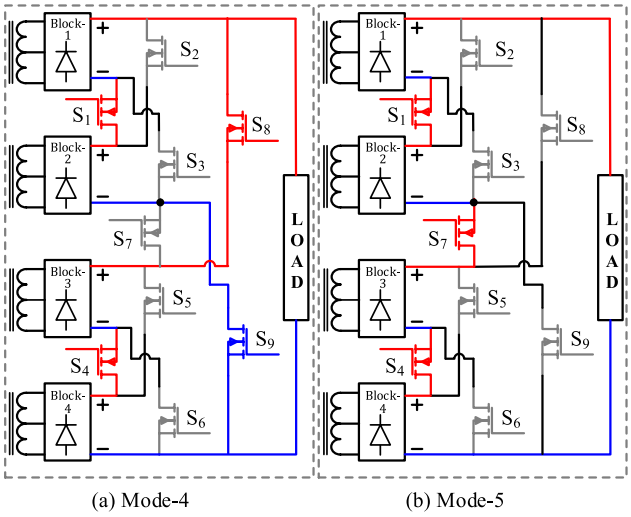

FIGURE 6. Status of switches in the output control section, (a) mode-4, (b) mode-5.

converter in mode-5 while the primary section is working in mode-1 is determined as

$$V_{out}(mode_{1/5}) = \left[2D_{eff}\frac{N_s}{N_p}\left(\frac{V_{in}}{2}\right)\right] \times 4 \tag{6}$$

V. DC GAIN OF THE CONVERTER

As discussed, the status of modes on both the input side and the output side determines the effective DC gain of the converter. Since each configuration connects circuit components differently, the gain of the converter also differs in each mode. By using (2), (4), (5) and (6), and configuring output blocks in mode-3 as a reference, the DC gain of the converter for each mode is determined as

$$G\_mode_{1/3} = \frac{V_{out}}{V_{in}} = \frac{N_s}{N_p}D_{eff} \tag{7}$$

$$G\_mode_{2/3} = \frac{V_{out}}{V_{in}} = \frac{1}{2}\frac{N_s}{N_p}D_{eff} \tag{8}$$

$$G\_mode_{1/4} = \frac{V_{out}}{V_{in}} = 2\frac{N_s}{N_p}D_{eff} \tag{9}$$

$$G\_mode_{1/5} = \frac{V_{out}}{V_{in}} = 4\frac{N_s}{N_p}D_{eff} \tag{10}$$

By using (7)-(10), comparison curves have been drawn for the normalized condition $N_s/N_p = 1$ in Fig. 7. As seen, the gain of mode-1/3 is double the gain of mode-2/3 and is four times higher in mode-1/5. The gain multiplication factor for each input/output configuration is listed in Table 1, where the gain can be raised to 4. By referring the gain = 1 to mode-2/3, the gain of the converter can be raised to 8 when it is configured to mode-1/5.

The gain characteristics of both input modes 1-2 can together be used to extend the range of the input voltage. A comparison plot of duty cycle against the variation of input voltage in mode-1/3 and mode-2/3 for the normalized conditions $N_s/N_p = 1$ is plotted in Fig. 8. The reduction

TABLE 1. Multiplication factors for the calculation of the gain of the converter in each configuration.

Status of primary section	Status of output control section	Gain multiple
Mode-1	Mode-3	1
	Mode-4	2
	Mode-5	4
Mode-2	Mode.3	0.5
	Mode-4	1
	Mode-5	2

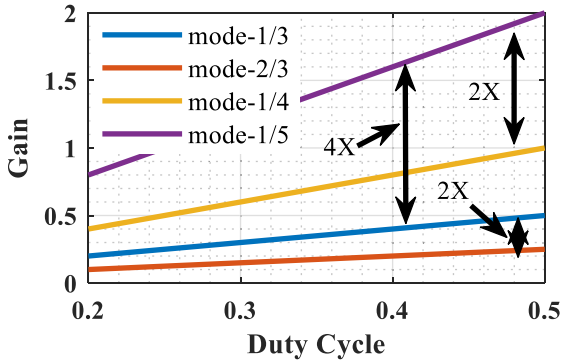

FIGURE 7. Comparison plot of gain of the converter in each mode by taking mode-1/3 as a reference.

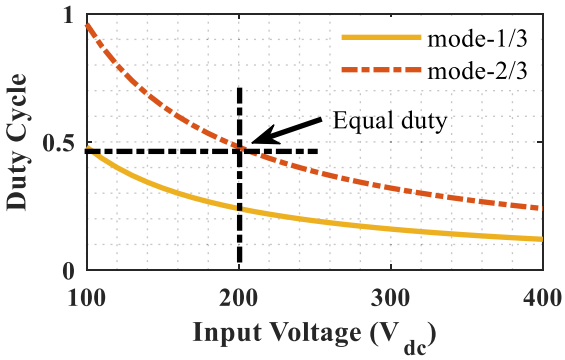

FIGURE 8. Comparison plot of the variation of duty cycle against the input voltage between mode-1/3 and mode-2/3, the reduced effective gain in mode-2/3 allows higher duty cycle.

of effective gain of the converter in mode-2/3 doubles the required duty cycle. This makes it possible to extend the input range while keeping the duty cycle high. For example, a converter can be set to operate in mode-1/3 for V_{in} = 100-200V and then to mode-2/3 above 200V. This keeps the duty cycle high for a wider range of input voltage.

VI. DESIGN CONSIDERATIONS

The circuit parameters of the converter act differently in each mode. Some important considerations for the stable operation of the converter have been outlined in the following:

A. TRANSFORMER CONSIDERATIONS

The combined effective parameters of all four transformers differ in each mode. Assuming that the output

TABLE 2. Logical table for the selection of output modes.

Output Mode	Switch Status								
	S_1	S_2	S_3	S_4	S_5	S_6	S_7	S_8	S_9
3	0	1	1	0	1	1	0	1	1
4	1	0	0	1	0	0	0	1	1
5	1	0	0	1	0	0	1	0	0

blocks are configured as default, the transformer parameters seen by the primary section in mode-1/3 are $L_{M\_P} = \{(L_{m1} + L_{m2}) \parallel (L_{m3} + L_{m4})\}$ and $L_{k\_P} = \{L_{k12} \parallel L_{k34}$, whereas in mode-2/3, it becomes $L_{M\_eq} = \{L_{m1}+L_{m2}+L_{m3}+L_{m4}$, $L_{k\_eq} = \{L_{k1} + L_{k2} + L_{k3} + L_{k4}$. The total magnetizing inductance of the circuit is four times less in mode-1/3 than in mode-2/3. Therefore, the magnetizing current would also be high in mode-1/3. The other parameters, like leakage inductance and resistance of the winding, will also display a similar pattern.

B. CURRENT CONSIDERATIONS

In mode-1/3, the stress on leg-2 is twice as much as the stress on the other two legs. This is because the sum of current flowing through the other two legs passes through leg-2. Therefore, the selection of power devices should be made by considering current/power stress in mode-1. On the secondary side, for the default mode-3, the total load current is shared between all four blocks, which makes stress on synchronous devices and filter element as $I_0/4$, in mode-4 as $I_0/2$, and it is I_0 in mode-5. The specifications of the secondary side elements can be chosen depending on the requirements of the intended application.

C. CONSIDERATION OF THE OUTPUT CONTROL SECTION

There are two very important considerations for the proper function of the output control section. One is the orientation of switches and the other is the electrical isolation of switches from each other. The switches should be placed such that there is no interference from body diodes as long as the switch is inactive. To ensure the isolation of each switch, the gate drive and the biasing supply need to be carefully managed. To verify the concept, this proposal uses TOSHIBA's photo-coupler part number TLP701 as a gate driver to the switches. Table 2 explains the control signals in terms of logical value to achieve respective mode on the output side.

D. CONTROL STRATEGY

A simplified control scheme has been implemented to validate the concept. There are three main sections of the scheme, one is sensing of the line voltage to adapt the required mode on the input side, the second is the mode selection on the output side and finally, the pulse width modulated control to regulate the converter. Since the circuit effective parameters differ in each operational mode, therefore, separate look-up tables for each combination of input/output modes have been implemented in the microprocessor. Based on the status of input/output mode, an appropriate control strategy along with voltage feedback has been adopted to control the converter. The complete control strategy has been implemented by using Microchip's dsPIC based microprocessor. To switch control signals between six power devices, PWM signals have been routed through six multiplexes. In order to remotely control the features, communication between the converter and the personal computer (PC) has also been implemented.

TABLE 3. Specification/component details of the example application.

Symbol	Quantity	Value
V_{in}	Input voltage range	100-400V_{dc}
	Mode-1	100-200V_{dc}
	Mode-2	>200V
V_{out}	Output voltage	12V_{dc}
P_{out}	Load power	1kW
f_s	Switching frequency	200 kHz
S_a-S_f	Power devices	GS66508B
	Gate driver	LM5114
	Synchronous MOSFET	BSC350N20
	Synchronous controller	ZXGD3107
Controller	Microchip's dsPIC	Dspic33fj16gs
Transformer	Core shape/ size/ material	PQ 20/20/3C95
L_p/L_s	Pri/ Sec inductance	190/3 µH
L_{kp}/L_{ks}	Pri/ Sec leakage inductance	2.8/0.05 µH
Rac	Pri/ Sec winding AC resistance	120/10 mΩ
N_p:N_s:N_s	Primary to secondary turn ratio	2:1:1
L_o	Output filter inductor	4.7 µH
C_0	Output filter capacitor	68 µF
S_1-S_9	Output control switches	SIR872A

E. CONSIDERATIONS OF MODE SWITCHOVER

The smooth transition between modes also requires a few considerations. On the primary side, the devices of the common leg turn ON/OFF during transition from mode-1 to mode-2 and vice versa. As discussed earlier, the gate drive signals are swapped between legs; an incorrect timing of the signals may destroy the devices. A short blanking time can be introduced in the controller to ensure the correct timing and phase of the signals. During transition, the converter resets effective gain from high to low and vice versa, the operational duty of the converter varies, which may result in instability. The strategy adopted for the evaluation of the concept is shown in Fig. 9, where the line voltage is sensed and the controller enters into a transition strategy. A delay of 15 μsec has been introduced between the switchovers to ensure the demagnetization of transformers, even for the worst case, such as light load. To keep the output voltage stable, the new duty cycle has been updated one cycle earlier than the start of the switchover command. On the secondary side, the switches of the output control section have to withstand abrupt turn ON during switchover of modes 3-5. The turn ON/OFF timing of switches in the loop also needs careful adjustment.

F. LOSS CONSIDERATIONS

For the evaluation of the performance, the proposed concept has been implemented in an example application of a PSFB

TABLE 4. Set of equations along with loss contribution of key components in each mode.

Status of I/P	Part	Loss	Loss calculation with respect to the status of output section		
			Mode-3	Mode-4	Mode-5
Mode-1	Power devices	Driver	$P_{dr} = (V_{gs}Q_g f) \times 6$	$P_{dr} = (V_{gs}Q_g f) \times 6$	$P_{dr} = (V_{gs}Q_g f) \times 6$
		Conduction	$P_{cond} = (I_{rms}^2\ R_{ds}) \times 3$	$P_{cond} = (I_{rms}^2\ R_{ds}) \times 3$	$P_{cond} = (I_{rms}^2\ R_{ds}) \times 3$
		Switching	$P_{sw} = (V_{in}I_{rms}f(t_{rise} + t_{fall})) \times 3$	$P_{sw} = (V_{in}I_{rms}f(t_{rise} + t_{fall})) \times 3$	$P_{sw} = (V_{in}I_{rms}f(t_{rise} + t_{fall})) \times 3$
	Synch. Devices	Conduction	$P_D = \left(\frac{1}{2}V_f I_o + I_{Srms}^2 R_D\right) \times 8$	$P_D = \left(\frac{1}{2}V_f I_o + I_{Srms}^2 R_D\right) \times 8$	$P_D = \left(\frac{1}{2}V_f I_o + I_{Srms}^2 R_D\right) \times 8$
	Active switches	Conduction	$(I_{Srms}^2 R_{dc}) \times 6$	$(I_{Srms}^2 R_{dc}) \times 4$	$(I_{Srms}^2 R_{dc}) \times 3$
	Transformer	Copper	$P_{cu} = (I_{rms}^2\ R_{ac} + I_{Srms}^2\ R_{Sac}) \times 4$	$P_{cu} = (I_{rms}^2\ R_{ac} + I_{Srms}^2\ R_{Sac}) \times 4$	$P_{cu} = (I_{rms}^2\ R_{ac} + I_{Srms}^2\ R_{Sac}) \times 4$
		Core	$P_c = (K_{fe}B^{\beta}V_e) \times 4$	$P_c = (K_{fe}B^{\beta}V_e) \times 4$	$P_c = (K_{fe}B^{\beta}V_e) \times 4$
Mode-2	Power devices	Driver	$P_{dr} = (V_{gs}Q_g f) \times 4$	$P_{dr} = (V_{gs}Q_g f) \times 4$	$P_{dr} = (V_{gs}Q_g f) \times 4$
		Conduction	$P_{cond} = (I_{rms}^2\ R_{ds}) \times 2$	$P_{cond} = (I_{rms}^2\ R_{ds}) \times 2$	$P_{cond} = (I_{rms}^2\ R_{ds}) \times 2$
		Switching	$P_{sw} = (V_{in}I_{rms}f(t_{rise} + t_{fall})) \times 2$	$P_{sw} = (V_{in}I_{rms}f(t_{rise} + t_{fall})) \times 2$	$P_{sw} = (V_{in}I_{rms}f(t_{rise} + t_{fall})) \times 2$
	Synch. Devices	Conduction	$P_D = \left(\frac{1}{2}V_f I_o + I_{Srms}^2 R_D\right) \times 8$	$P_D = \left(\frac{1}{2}V_f I_o + I_{Srms}^2 R_D\right) \times 8$	$P_D = \left(\frac{1}{2}V_f I_o + I_{Srms}^2 R_D\right) \times 8$
	Active switches	Conduction	$(I_{Srms}^2 R_{dc}) \times 6$	$(I_{Srms}^2 R_{dc}) \times 4$	$(I_{Srms}^2 R_{dc}) \times 3$
	Transformer	Copper	$P_{cu} = (I_{rms}^2\ R_{ac} + I_{Srms}^2\ R_{Sac}) \times 4$	$P_{cu} = (I_{rms}^2\ R_{ac} + I_{Srms}^2\ R_{Sac}) \times 4$	$P_{cu} = (I_{rms}^2\ R_{ac} + I_{Srms}^2\ R_{Sac}) \times 4$
		Core	$P_c = (K_{fe}B^{\beta}V_e) \times 4$	$P_c = (K_{fe}B^{\beta}V_e) \times 4$	$P_c = (K_{fe}B^{\beta}V_e) \times 4$

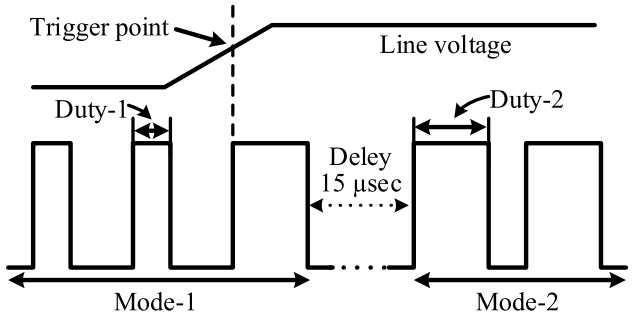

FIGURE 9. Control strategy for the smooth switchover of primary modes 1 and 2.

converter. The specifications of the converter along with details of the circuit elements are listed in Table-3.

A standard set of equations, like core loss, switching loss, gate driver loss, conduction loss and copper loss has been written on a math processor for analytical estimation of losses in each mode. The equations along with loss contribution of key components in each mode is shown in Table 4. The component-specific parameters have been taken from the manufacturer datasheets. The remaining key parameters, such as the transformer's AC resistance of the windings, leakage inductance and magnetizing inductance have been measured by using an impedance analyzer. For the example application, the converter is configured to operate in mode-1/3 for $V_{in} = 100 - 200V$, above $200V$ it operates in mode-2/3. The losses are calculated separately for both input modes and by the switching output modes from 3-5.

The total converter loss in each mode is compared in Fig. 10, which shows similar characteristics. The losses are maximum for the primary/secondary configuration of mode-1/mode-3, where the maximum number of power devices and output control switches are involved, and results in maximum switching and conduction losses. As a comparison between mode-1/mode-3 and mode-1/mode-5, the conduction losses are less in the latter because of the high voltage/low current conditions. As the output voltage increases, current decreases, which decreases conduction losses. For the comparison between mode-1 and mode-2, the performance shows better characteristics in mode-2, because the devices of leg-2 remain OFF. Although the input voltage is higher in mode-2, the number of series-connected transformers becomes double that of mode-1, which reduces the applied voltage to the transformers by four.

G. COMPARISON WITH CONVENTIONAL CONVERTERS

As mentioned, this work proposes a unique single approach to extend both the input range and the output range. An exact cost/performance comparison between the proposed and the conventional approaches is difficult to make. However, a generalized analytical comparison of key parameters for the same specifications is given in Table 5. For wide input range applications, the higher operational duty cycle in the proposed converter maintains the performance stable. The operation with a higher duty cycle reduces ringing and overshoot; as a result, EMI characteristics improve. The only

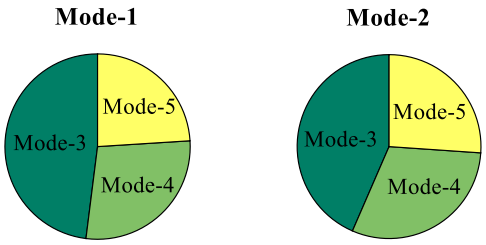

FIGURE 10. Loss comparison of the working of the converter in all three output modes against both the input modes at load power of 1kW.

TABLE 5. Generalized performance comparison of key parameters between the proposed converter and the conventional converter.

Quantity	Conventional converter	Proposed converter
Flow of circulation current in a half-cycle time at Vin (max.)	75%	50%
Switching/conduction loss	100%	150%
Duty cycle at Vin (max.)	10%	25%
Stress on synchronous devices	100%	25%
Stress on filtering elements	100%	25%
Thermal management	Complex	Simple
Switching frequency	Variable	Fixed
EMI	High	Low
Efficiency against input voltage	Degrading	Stable
Efficiency against output voltage	Degrading	Stable
Single solution to extend both input and output ranges together	No	Yes
Active switches on the output	0%	100%
Design complexity	Less	High

difference is the addition of two more power devices on the primary side, which slightly increases conduction and switching losses in the proposed concept. Similarly, for wide output range applications, unlike the conventional approach, the proposed converter extends the range while keeping the switching frequency constant. This simplifies the design and selection of input/output filtering components. In addition, it also improves EMI performance. Although the proposal uses active switches to extend the range, which adds additional conduction losses, it could be maintained at an acceptable range by choosing appropriate switches following the requirements of the intended application. As a whole, the part count in the proposed converter is higher than the conventional, which increases complexity; however, the reduced stress on circuit parts cuts the power rating and volume of the components. The cost of components mainly depends on the power/stress levels; the only available option in certain cases is a customized solution [27], [28]. For example, compared with the conventional approach for the same specifications, the DC-current requirement of the filtering components is greater than 50 Amps. The market for such a high-current component is slim; the only solution available

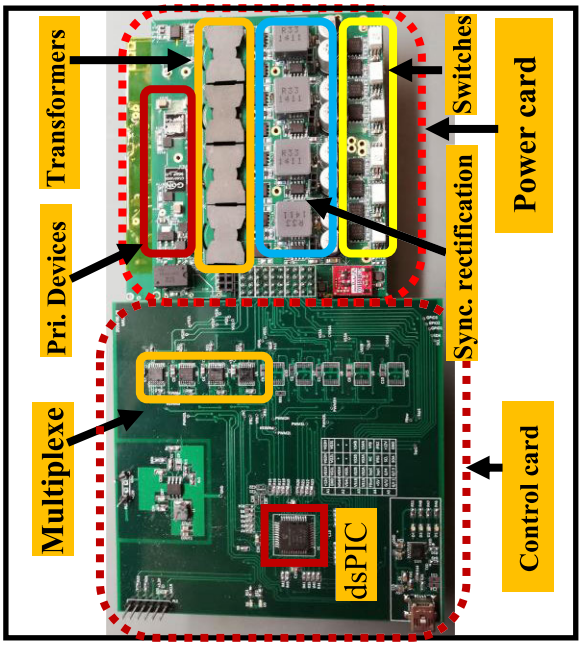

FIGURE 11. Picture of the prototype, showing both the control card and the power card.

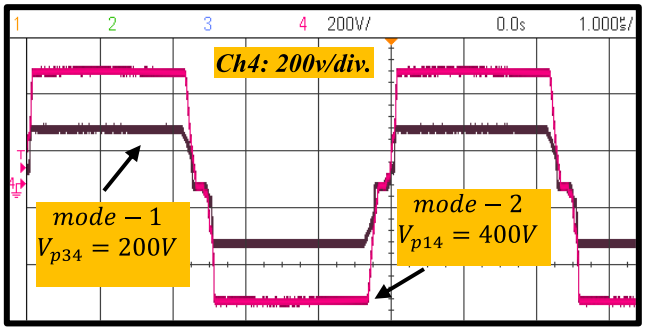

FIGURE 12. Demonstration of the equal operational duty both in mode-1/mode-3 and mode-2/mode-3, although the change in the input voltage is 100%.

is either arranging parallel elements or customizing. This becomes even more difficult to find solutions as the power level increases [27]. Furthermore, the presented flexible single solution can be remotely configured to meet a variety of applications. In addition, the use of several transformers and parallel operation of secondary circuit elements in the proposal reduces thermal management efforts as well as better system reliability.

VII. EXPERIMENTAL INVESTIGATIONS

A prototype of the example application has been designed to verify the proposed concept. The specifications and component details have already been listed in Table-3. As shown in Fig. 11, the prototype consists of two modules, one for the power section and the other for the control section. The control of the converter is based on Microchip's dsPIC platform. The control signals are cloned by using multiplexers. As given, the physical turn ratio N_p/N_s of a single

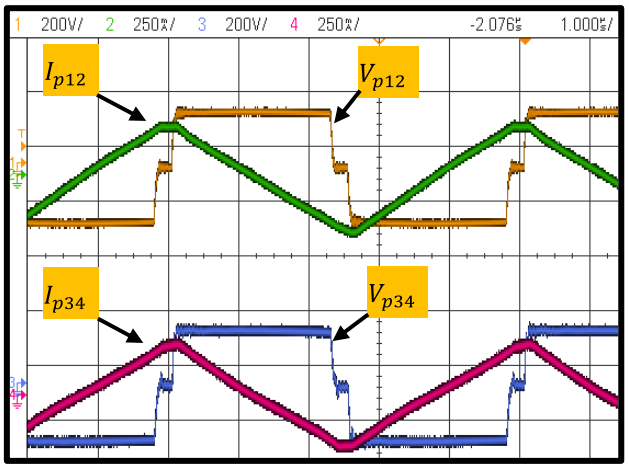

FIGURE 13. Demonstration of the equal amount of flow of primary current in mode-1 through two different paths. Ch1:-200V/div, Ch 2:-250mA/div, Ch 3:-200V/div, Ch 4:-250mA/div Time base:-1μ sec/div.

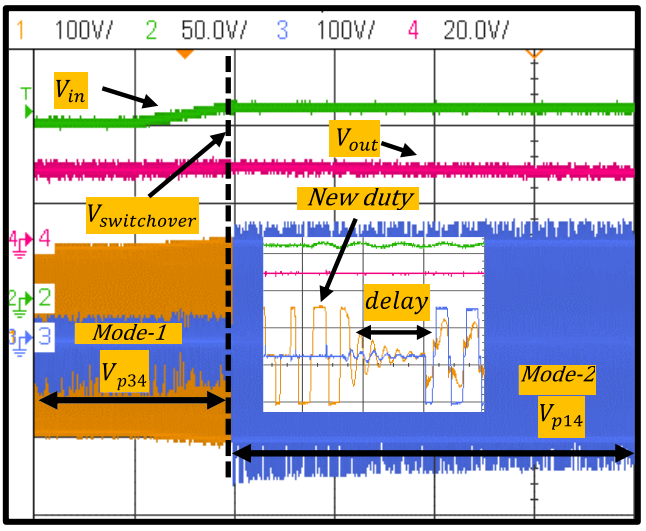

FIGURE 14. Dynamic transition of converter from mode-1/3 to mode-2/3. Ch 1:-100V/div, Ch 2:- 50V/div, Ch 3:- 100V/div, Ch 4:- 20V/div.

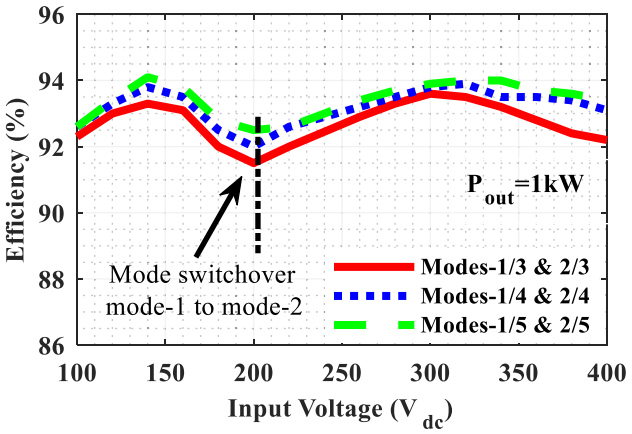

FIGURE 15. Demonstration of the stable performance of the converter over the complete range of input voltage at fixed load power by using both input modes separately for each operational output mode.

center-tapped transformer is 2:1:1. By using (2) and (4), the effective DC conversion ratio of mode-1/mode-3 is 4:1:1, it changes to 8:1:1 in mode-2/mode-3. The performance has been investigated for all possible operational modes. For simplicity, the extended range of both the input side and the output side has been discussed separately.

A. EXTENSION OF INPUT RANGE

As discussed, the range of the input voltage can be extended by reconfiguring the converter between mode-1/mode-3 and mode-2/mode-3. The reduction of gain by half in mode-2/mode-3 allows the converter to operate with higher operational duty at high input voltage. This is demonstrated in Fig. 12, where the transformer bridge voltage has been compared for the operation of the converter in both modes. As seen, the duty cycle in both modes remains the same despite the change in input voltage from 200V to 400V. The operation with a high duty cycle minimizes the freewheeling interval, therefore, circulating current flows for less time, which keeps the performance stable.

It has already been mentioned that in mode-1/mode-3 all three legs on the input side are active, the primary current divides equally into two paths. That is, primary current I_{p12} through transformers T_1-T_2 and primary current I_{p34} through transformers T_3-T_4. Fig. 13 demonstrates the bridge voltage along with the respective primary current for both paths, i.e., V_{12}/I_{p12} and V_{34}/I_{p34}. As seen, both paths bear the same level of voltage and current. Both of these currents add up in the common leg, which makes the stress two times higher for this leg.

Fig. 14 demonstrates the dynamic switchover of the converter from mode-1/3 to mode-2/3. The transformer bridge voltage for both operational modes has been simultaneously captured along with the input voltage and the output voltage of the converter. The figure shows both the actual waveforms captured at the trigger level of the oscilloscope along with the embedded magnified view at the instance of transition. As soon as the line voltage reaches the pre-set mode trigger voltage, the microprocessor updates the operational duty and adds a delay before switching to another mode. Decaying oscillations during the delay interval ensures demagnetization of cores before switchover.

Fig. 15 demonstrates the stable efficiency characteristics of the converter over the complete range of the input voltage at P_{out} = 1kW. The investigations have been made separately for all three output modes. To maintain performance stable, the converter switches between two input modes. As seen, the converter operates in mode-1/mode-3, mode-1/mode-4, and mode-1/mode-5 for V_{in} = 100-200V; as the input voltage increases the efficiency drops because of the reduced duty cycle. For V_{in} > 200V, the converter reconfigures to mode-2/mode-3, mode-2/mode-4, and mode-2/mode-5 respectively. This consequently rearranges the operational duty cycle to high again, which results in improved efficiency over the complete range of input voltage.

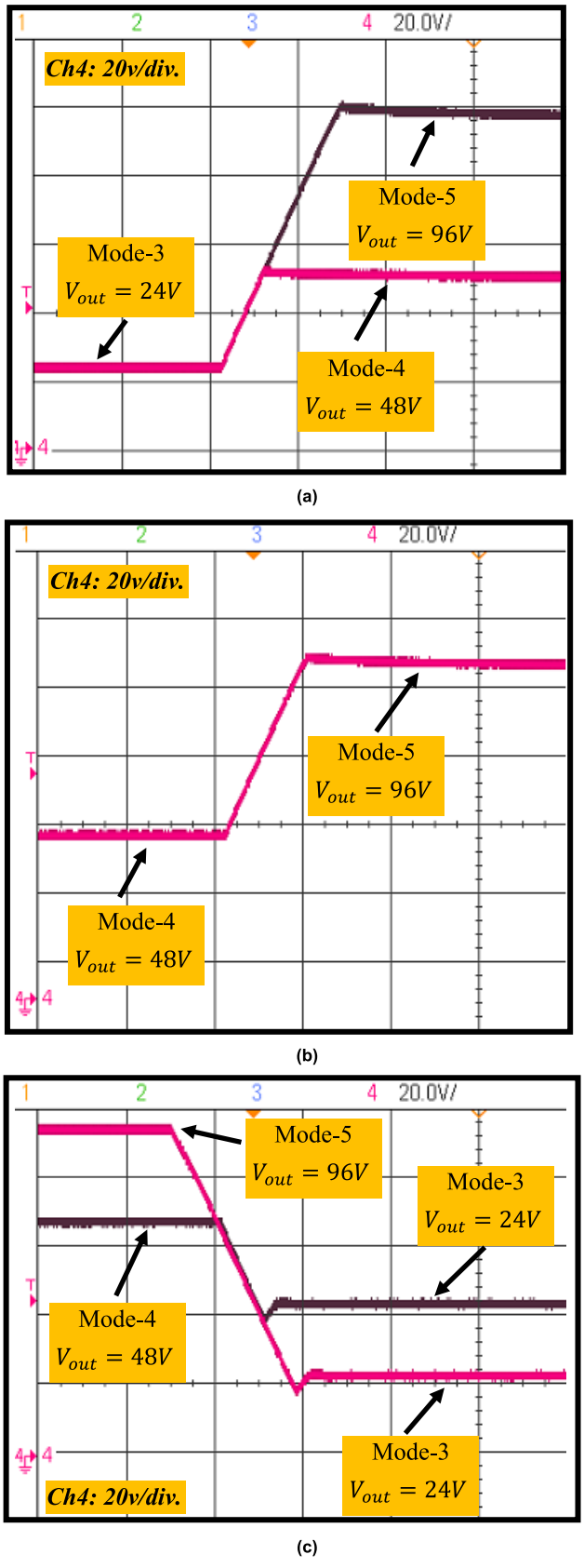

FIGURE 16. Dynamic transition of the output control section (a) mode-3 to mode-4 and mode-3 to mode-5, (b) mode-4 to mode-5, (c) mode-4 to mode-3 and mode-5 to mode-3.

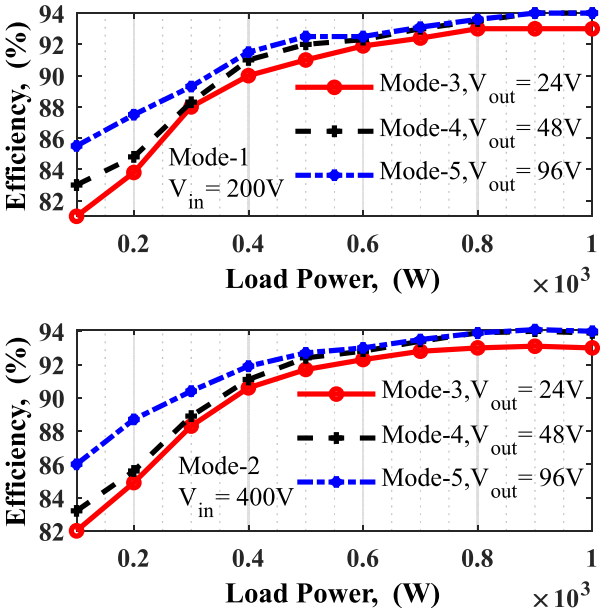

FIGURE 17. Comparison of the performance of the converter for the three output modes 3-5 against both the input modes and for the variation in the load power.

B. EXTENSION OF OUTPUT RANGE

The performance of all three output modes, i.e., mode-3 to mode-5, has been characterized separately against both input modes. Figures 16(a)-16(c) show the dynamic switchover of output modes by keeping the status of the input side unchanged. Fig. 16(a) demonstrates the switchover from mode-3 to mode-4 and from mode-3 to mode-5. As mentioned, in mode-3, all output blocks act as all-parallel with the base output voltage of $V_{out} = 24V$. Similarly, mode-4 arranges the two first in series then in parallel. This raises the output voltage to $V_{out} = 48V$. Finally, mode-5 arranges all four blocks in series, which in turn raises the output voltage to $V_{out} = 96V$. Fig. 16(b) demonstrates the switchover from mode-3 to mode-5, whereas Fig. 16(c) demonstrates the switchover in reverse order, that is from mode-5 to mode-3 and mode-4. For greater legibility, the ground reference of the waveform from mode-4 to mode-3 in Fig. 16 (c) is shifted from the level shown.

Similar to the analytical loss analysis, the efficiency of the converter is recorded separately for both input modes and for each configuration of the output control section. A comparison is shown in Fig. 17. The comparison shows similar characteristics as previously discussed. The involvement of more devices in mode-1/mode-3 shows slightly higher losses than in mode-2/mode-3. Similarly, the use of more switches in mode-3 slightly reduces efficiency compared to mode-4 and mode-5.

VIII. CONCLUSION

The proposed concept has been successfully demonstrated in an example application of a power converter. It demonstrates stable efficiency over the wide range of both input

voltage and output voltage. Two reconfigurable modes on the input side and three reconfigurable modes on the output side can together raise the gain to eight. The presented flexible approach can be applied in a variety of applications, where either an extended range of the input or output is a requirement. For wide input and constant output voltage applications, the performance of the converter can be optimized by using two input modes. Similarly, for wide output applications or applications where the system must start with low voltage and high current or vice versa, the three reconfigurable modes on the output side can meet this requirement. The flexible structure further simplifies the deployment of one design in other applications by programming it to a new specification either by configuring it manually or by pre-programming. By using a flexible reconfigurable structure, the output voltage can also be adjusted depending on the loading conditions, like low voltage/high current to high voltage/low current. In addition, the use of several transformers shares the load power among multiple elements on the secondary side, which allows the use of low-profile elements and simplifies heat management. This can further help to build low-profile power converters to meet the requirement of the present space-conscious industry. As a part of future work, an adaptive control strategy is planned to further optimize the performance of the converter.

REFERENCES

[1] Y. Lu, H. Wu, B. Tu, M. Li, Y. Xia, and Y. Xing, "Ultra-wide output voltage range power supply based on modular switched-converter principle," *IEEE Trans. Power Electron.*, vol. 35, no. 1, pp. 94–106, Jan. 2020, doi: 10.1109/TPEL.2019.2912724.

[2] P. Sun, L. Zhou, and K. M. Smedley, "A reconfigurable structure DC–DC converter with wide output range and constant peak power," *IEEE Trans. Power Electron.*, vol. 26, no. 10, pp. 2925–2935, Oct. 2011, doi: 10.1109/TPEL.2011.2129576.

[3] Z. Li, B. Xue, and H. Wang, "An interleaved secondary-side modulated LLC resonant converter for wide output range applications," *IEEE Trans. Ind. Electron.*, vol. 67, no. 2, pp. 1124–1135, Feb. 2020, doi: 10.1109/TIE.2019.2897507.

[4] H. Wang, M. Shang, and D. Shu, "Design considerations of efficiency enhanced LLC PEV charger using reconfigurable transformer," *IEEE Trans. Veh. Technol.*, vol. 68, no. 9, pp. 8642–8651, Sep. 2019, doi: 10.1109/TVT.2019.2930551.

[5] H. Wu, K. Sun, R. Chen, H. Hu, and Y. Xing, "Full-bridge three-port converters with wide input voltage range for renewable power systems," *IEEE Trans. Power Electron.*, vol. 27, no. 9, pp. 3965–3974, Sep. 2012, doi: 10.1109/TPEL.2012.2188105.

[6] A. Chub, D. Vinnikov, R. Kosenko, and E. Liivik, "Wide input voltage range photovoltaic microconverter with reconfigurable buck–boost switching stage," *IEEE Trans. Ind. Electron.*, vol. 64, no. 7, pp. 5974–5983, Jul. 2017, doi: 10.1109/TIE.2016.2645891.

[7] Q. Cao, Z. Li, and H. Wang, "Wide voltage gain range LLC DC/DC topologies: State-of-the-art," in *Proc. Int. Power Electron. Conf. (IPEC-Niigata-ECCE Asia)*, May 2018, pp. 100–107, doi: 10.23919/IPEC.2018.8507899.

[8] D. Zhang and D. Zhang, "Flexible-structured phase-shifted multiple-full-bridge DC–DC power supply with wide range output," *IET Power Electron.*, vol. 9, no. 1, pp. 132–141, Jan. 2016, doi: 10.1049/iet-pel.2014.0657.

[9] B.-C. Kim, K.-B. Park, and G.-W. Moon, "Asymmetric PWM control scheme during hold-up time for LLC resonant converter," *IEEE Trans. Ind. Electron.*, vol. 59, no. 7, pp. 2992–2997, Jul. 2012, doi: 10.1109/TIE.2011.2166237.

[10] Y. Jang, M. M. Jovanovic, and D. L. Dillman, "Hold-up time extension circuit with integrated magnetics," *IEEE Trans. Power Electron.*, vol. 21, no. 2, pp. 394–400, Mar. 2006, doi: 10.1109/TPEL.2005.869750.

[11] I.-H. Cho, K.-M. Cho, J.-W. Kim, and G.-W. Moon, "A new phase-shifted full-bridge converter with maximum duty operation for server power system," *IEEE Trans. Power Electron.*, vol. 26, no. 12, pp. 3491–3500, Dec. 2011, doi: 10.1109/TPEL.2011.2129532.

[12] B. Yang, P. Xu, and F. C. Lee, "Range winding for wide input range front end DC/DC converter," in *Proc. 16th Annu. IEEE Appl. Power Electron. Conf. Expo. (APEC)*, vol. 1, Mar. 2001, pp. 476–479, doi: 10.1109/APEC.2001.911689.

[13] M. A. Bakar, M. F. Alam, A. Majid, and K. Bertilsson, "Dual-mode stable performance phase-shifted full-bridge converter for wide-input and medium-power applications," *IEEE Trans. Power Electron.*, vol. 36, no. 6, pp. 6375–6388, Jun. 2021, doi: 10.1109/TPEL.2020.3033386.

[14] B.-Y. Chen and Y.-S. Lai, "Switching control technique of phase-shift-controlled full-bridge converter to improve efficiency under light-load and standby conditions without additional auxiliary components," *IEEE Trans. Power Electron.*, vol. 25, no. 4, pp. 1001–1012, Apr. 2010, doi: 10.1109/TPEL.2009.2033069.

[15] G.-B. Koo, G.-W. Moon, and M.-J. Youn, "New zero-voltage-switching phase-shift full-bridge converter with low conduction losses," *IEEE Trans. Ind. Electron.*, vol. 52, no. 1, pp. 228–235, Feb. 2005, doi: 10.1109/TIE.2004.841063.

[16] D. Liu, Y. Wang, F. Deng, Q. Zhang, and Z. Chen, "Zero-voltage switching full-bridge T-type DC/DC converter with wide input voltage range and balanced switch currents," *IEEE Trans. Power Electron.*, vol. 33, no. 12, pp. 10449–10466, Dec. 2018, doi: 10.1109/TPEL.2018.2800902.

[17] H. Wu, X. Zhan, and Y. Xing, "Interleaved LLC resonant converter with hybrid rectifier and variable-frequency plus phase-shift control for wide output voltage range applications," *IEEE Trans. Power Electron.*, vol. 32, no. 6, pp. 4246–4257, Jun. 2017, doi: 10.1109/TPEL.2016.2602545.

[18] H. Wu, L. Chen, and Y. Xing, "Secondary-side phase-shift-controlled dual-transformer-based asymmetrical dual-bridge converter with wide voltage gain," *IEEE Trans. Power Electron.*, vol. 30, no. 10, pp. 5381–5392, Oct. 2015, doi: 10.1109/TPEL.2014.2371922.

[19] M. Kim, H. Jeong, B. Han, and S. Choi, "New parallel loaded resonant converter with wide output voltage range," *IEEE Trans. Power Electron.*, vol. 33, no. 4, pp. 3106–3114, Apr. 2018, doi: 10.1109/TPEL.2017.2706360.

[20] M. A. Bakar and K. Bertilsson, "A modified higher operational duty phase shifted full bridge converter for reduced circulation current," *IEEE Open J. Ind. Electron. Soc.*, vol. 1, pp. 82–96, 2020, doi: 10.1109/OJIES.2020.2994142.

[21] M. A. Bakar, F. Alam, M. Das, S. Barg, and K. Bertilsson, "Reconfigurable three state DC–DC power converter for the wide output range applications," in *Proc. 45th Annu. Conf. IEEE Ind. Electron. Soc. (IECON)*, vol. 1, Oct. 2019, pp. 4911–4916, doi: 10.1109/IECON.2019.8927652.

[22] G.-B. Koo, G.-W. Moon, and M.-J. Youn, "Analysis and design of phase shift full bridge converter with series-connected two transformers," *IEEE Trans. Power Electron.*, vol. 19, no. 2, pp. 411–419, Mar. 2004, doi: 10.1109/TPEL.2003.823193.

[23] R. Ayyanar and N. Mohan, "Novel soft-switching DC–DC converter with full ZVS-range and reduced filter requirement—Part II: Constant-input, variable-output applications," *IEEE Trans. Power Electron.*, vol. 16, no. 2, pp. 193–200, Mar. 2001, doi: 10.1109/63.911143.

[24] G. Chen, Y. Deng, J. Dong, Y. Hu, L. Jiang, and X. He, "Integrated multiple-output synchronous buck converter for electric vehicle power supply," *IEEE Trans. Veh. Technol.*, vol. 66, no. 7, pp. 5752–5761, Jul. 2017, doi: 10.1109/TVT.2016.2633068.

[25] W. Chen, X. Ruan, and R. Zhang, "A novel zero-voltage-switching PWM full bridge converter," *IEEE Trans. Power Electron.*, vol. 23, no. 2, pp. 793–801, Mar. 2008, doi: 10.1109/TPEL.2007.915764.

[26] G. Ning, W. Chen, L. Shu, and X. Qu, "A hybrid ZVZCS dual-transformer-based full-bridge converter operating in DCM for MVDC grids," *IEEE Trans. Power Electron.*, vol. 32, no. 7, pp. 5162–5170, Jul. 2017, doi: 10.1109/TPEL.2016.2604246.

[27] G. Domingues-Olavarria, P. Fyhr, A. Reinap, M. Andersson, and M. Alakula, "From chip to converter: A complete cost model for power electronics converters," *IEEE Trans. Power Electron.*, vol. 32, no. 11, pp. 8681–8692, Nov. 2017, doi: 10.1109/TPEL.2017.2651407.

[28] P. Tu, S. Yang, and P. Wang, "Reliability and cost based redundancy design for modular multilevel converter," *IEEE Trans. Ind. Electron.*, vol. 66, no. 3, pp. 2333–2342, Mar. 2019, doi: 10.1109/TIE.2018.2793263.

M. ABU BAKAR received the M.S. degree, in 2012 and the Ph.D. degree, in power electronics from Mid Sweden University, Sweden, in 2020. He is currently doing research and development for Powerbox International AB, Sweden. He has years of industrial experience designing a customized solution related to electrical and electronics engineering. His research interests include power electronics, and analog, and digital electronics

M. FARHAN ALAM received the B.S. degree in electronics from Air University Islamabad Pakistan, in 2007, and the M.S. degree in electronics from Mid Sweden University, Sweden, in 2012. From 2012 to 2016, he worked as a Design Engineer with SEPS AB Sundsvall Sweden, where he worked in high frequency GaN power converters and designing, as an Electronic Marker Locator. Since 2016, he has been a Research Assistant with Mid Sweden University in the power electronics group. His research interests include the development of a microcontroller system designing PCB for power converters testing and characterization of power converters.

MATS WÅRDEMARK received the M.Sc. degree in electronics from the Royal Institute of Technology, Stockholm, Sweden, in 1995. From 1995 to 2002, he worked with designing custom power supplies for the telecom market, Ericsson. Since 2002, he has been working with Powerbox AB, where he worked on design and development of power supplies for telecom, medical, and industrial applications. He involved in several wide band gap research projects together with Mid University in Sundsvall, Uppsala University, and RISE Research Institutes, Sweden.

KENT BERTILSSON (Member, IEEE) received the M.Sc. degree in electronics from Mid Sweden University, Sundsvall, Sweden, in 1999, and the Ph.D. degree, in device design and optimization of silicon carbide devices from the Royal Institute of Technology, Stockholm, Sweden, in 2005. Since 2005, he has been leading the research in power electronics with Mid Sweden University, where he is currently a Full Professor. In 2009, he co-founded SEPS Technologies AB, Sundsvall, where he is the CEO. He has authored or coauthored more than 60 articles in international journals and conferences in the fields of semiconductor device simulations, silicon carbide devices, detectors, and power electronics.